Extrusion-based 3D printing of oral solid dosage forms : material requirements and equipment dependencies

Extrusion-based 3D printing of oral solid dosage forms: material requirements and equipment dependencies.

Henry S.[a], Samaro A.[a], Marchesini, F.H.[b], Shaqour B.[c,d], Macedo J.[e], Vanhoorne V.[a], Vervaet C.[a,*]

[a] *Laboratory of Pharmaceutical Technology, Ghent University, 9000 Ghent, Belgium*
[b] *Department of Materials, Textiles and Chemical Engineering, Ghent University, 9052 Zwijnaarde, Belgium*
[c] *Voxdale bv, Bijkhoevelaan 32C, 2110 Wijnegem, Belgium*
[d] *Laboratory for Microbiology, Parasitology and Hygiene (LMPH), Faculty of Pharmaceutical, Biomedical and Veterinary Sciences, University of Antwerp, Universiteitsplein 1 S.7, 2610 Antwerp, Belgium*
[e] *iMed.ULisboa, Faculdade de Farmácia, Universidade de Lisboa, Lisboa, Portugal*

Abstract

Extrusion-based 3D printing is steadily gaining importance as a manufacturing technique due to its flexibility and wide range of possible end-products. In the medical field, the technique is being exploited for a variety of applications and one of these is the production of personalised medicines. However, despite many proof-of-concept studies, more thorough insights in the production technique itself and the required material properties are needed before 3D printing can be fully exploited in a hospital or pharmacy setting. This research aims at clarifying the complex interplay between material properties, process parameters and printer-dependent variables. A variety of different polymers and polymer-drug blends were extruded (diameter 1.75±0.05 mm) and characterised in terms of mechanical, thermal and rheological properties. These properties, together with the processing temperature, printing speeds and different nozzle diameters of the 3D printer were linked to the quality of the end-product. Different failure mechanisms (mechanical, thermal) were assessed. Decisive material parameters (e.g. cross-over point) for optimal printing behaviour and the importance of printer construction (nozzle diameter) were clarified. In general, this study offers insight into the 3D printing process and will help to speed up future pharmaceutical formulation development for printlets.

Keywords: Fused deposition modeling, 3D printing, Rheology, Mechanical analysis, Thermal analysis, Extrusion

1. Introduction

Nowadays, medical treatment is mostly based on the one-size-fits-all approach where mass-produced medicines contain a dose suitable for the majority of the population. However, due to patient variability in terms of e.g. gender, genetics or weight, there is an increasing interest in dose personalisation. The ability to produce a personalised dosage form on-demand requires however a flexible manufacturing technique. Established pharmaceutical manufacturing techniques are cost-effective for large-scale production

*Corresponding author
Email address: Chris.Vervaet@UGent.be (Vervaet C.)

but are dose inflexible. On the contrary, extrusion-based 3D printing is cost- and time-efficient on a small scale.[1] Apart from mere dose personalisation, extrusion-based 3D printing can even be used to produce tablets containing multiple APIs, each in patient-tailored concentrations.[2]

The terms “3D printing” or "rapid prototyping" are collective terms for a variety of techniques, which can be classified in seven categories according to the American Society for Testing and Materials (ASTM) group: (1) vat photopolymerisation, (2) binder jet printing, (3) material jet printing, (4) powder bed fusion, (5) directed energy deposition, (6) sheet lamination and (7) material extrusion.[3] Extrusion-based 3D printing or fused deposition modelling (FDM) is classified in this last category and is one of the most popular techniques, due to its fast production speed and cost-effectiveness. In extrusion-based 3D printing, a filament consisting of a polymer matrix and embedded drug is fed by roller grips to a heated nozzle. Within this nozzle, the filament softens and is deposited on a bed. Either the nozzle or bed can move into different axes to create a 3D object.[4] The prerequisites for this type of manufacturing are excellent flow properties within the nozzle and fast hardening of the polymer upon cooling on the bed.[5] The drug-loaded feedstock material for this FDM technique is produced by either soaking the previously prepared filament into a drug solution or performing hot melt extrusion (HME) with physical mixtures. The soaking method is an outdated, inefficient technique which has the disadvantage that the achievable drug load is minimal and few commercial filaments are pharmaceutically approved. On the contrary, the HME method can rapidly produce homogeneous blends with high drug load. The drawback of HME is however the necessity for heating, which excludes the use of active pharmaceutical ingredients (API) prone to thermal degradation.[6] The combination of HME with FDM has been used successfully in academic research to manufacture a variety of dosage forms e.g. oral thin films, controlled or immediate release tablets, subdermal implants, intrauterine systems or wound dressings.[3]

Despite the extensive academic research and many proof-of-concept studies, more thorough insights into the different processing steps of FDM 3D printing are required before the technique can be implemented to produce personalised dosage forms. The main steps in the 3D printing process are (1) filament production, (2) filament feeding, (3) deposition and (4) solidification on the build platform.[7] During filament production by HME, special attention should be paid to diameter correctness and consistency as the filament diameter is a critical quality attribute in the FDM 3D printing process. Smaller filaments might not withstand the stresses exerted by the gears, while larger filaments might clog the PTFE-tube and impede transport to the liquefying zone. The diameter consistency is not only important to ensure a proper printing process, but also ensures content and mass uniformity of pharmaceutical dosage forms.[8] During filament feeding, a rotating roller feeds the filament through a PTFE-tube to the heater block and nozzle, where the filament melts. (Fig. S1) The solid filament above this liquefied zone acts as a piston which extrudes the molten polymer out of the nozzle.[9] The feed rate, material properties and heat flux determine the amount of molten material within the heated zone. A higher temperature generally improves flow out of the nozzle by reducing the viscosity of the molten polymer and thus the pressure drop over the printer head. It also enhances the adhesion between successive layers. Increasing the temperature of the process too much might however induce polymer degradation, residues on the melt channel or a deformed end-product.[4,10]

In general, a better understanding of the required material properties for FDM 3D printing is necessary to print accurate dosage forms in terms of surface area, shape and weight and is of major interest to enable its use at the point-of-care locations.[7,11] Expanding the portfolio of polymers suitable for FDM 3D printing would also be beneficial for pharmaceutical printing as currently implemented polymers are mainly used in spare parts production (e.g. aerospace, automotive or maritime industries).[9,12] At the moment, the production of 3D printed dosage forms is however still an empirical process which requires a huge time investment to screen and adapt different formulations according to the trial-and-error principle, especially for researchers new to the field.[13] It is known that material properties of the filaments greatly impact the printability and determine the window of process conditions.[14] Therefore, the optimal rheological, thermal and mechanical properties of the feedstock-material should be characterized, in combination with their ideal process settings to achieve a successful end-product. Recently, an artificial intelligence machine learning technique was developed to speed up the FDM development and production process by linking material parameters directly to printability outcomes using a large training set. The technique proved valuable to effectively predict process settings of drug-loaded filaments.[13] However, previous studies merely classify a filament as 'non-printable' or 'printable' with only limited rationale from a rheological point of view for this behaviour. Whenever a full rheological analysis is made, it is often limited to a small, specific group of polymers which impairs a broader applicability of the results. The importance of rheology on the efficient production of high quality end products was already shown to be vital in hot melt processes but is often underutilized.[15,7,16,17,18] Therefore, the aim of the present study was to focus on the causality of a variety of printing failures and linking these to simple mathematical equations describing the 3D printing process. Multiple key material properties which determine feed- and printability of pharmaceutical filaments and their processing window in a desktop FDM 3D printer were determined using a dedicated rheological, mechanical and thermal analysis of a variety of polymers. The study is intended to serve as a guide to speed up future filament development by identifying root causes of a printing failure and providing solutions to overcome these.

2. Materials and Methods

2.1. Materials

A variety of polymers was screened to investigate their window of feed- and printability. Thermoplastic polyurethanes (Tecoflex® EG-72D, Tecophilic® SP-60D-60 Tecophilic® SP-93A) (Lubrizol, Ohio, USA) and ethylene-vinyl-acetates (EVA1070, EVA2825A) (Celanese, UK) were processed as pellets. Polycaprolactone (CAPA 6506, Perstorp, UK), polyethylene-oxide (Polyox WSR N10, Dupont, Germany), polymethacrylates (Eudragit EPO, Evonik, Germany), hydroxy-propylcellulose (Klucel EF, Ashland, Switzerland), polyvinylcaprolactam–polyvinyl acetate–polyethylene glycol graft copolymer (Soluplus®,BASF, Germany) and copovidone (Kollidon VA64®, BASF, Germany) were processed as powder. From this list of polymers, the TPUs and CAPA6506 are at this moment not approved for pharmaceutical use in Europe. Black polylactic acid filament was purchased from 3D4Makers (Haarlem, Netherlands). Ibuprofen (SI group, USA) was added as active pharmaceutical ingredient (API) to Polyox WSR N10 (PEO N10) and polycaprolactone (PCL) in 20% (w/w) and 40% (w/w). Scotch blue painter's tape 50 mm was supplied by 3M (Bracknell, UK).

2.2. Filament Preparation: Hot Melt Extrusion

Pure polymers were extruded using a co-rotating, fully intermeshing twin-screw extruder (Prism Eurolab 16, Thermo Fisher, Germany) equipped with co-rotating twin screws and a custom-made heated die of 1.70 mm diameter. A DD flex-wall 18 feeder (Brabender, Germany) was used. Screw speed and feed rate were kept constant at 80 rpm and 0.3 kg/h, respectively. A standard screw configuration consisting of transporting elements, two kneading blocks and a discharge element were used.[19]

The processing range for hot melt extrusion of a specific polymer (blend) depends on its complex viscosity η^*, which should fall between 1,000 and 10,000 Pa.s. Within this range, the torque limit of the extruder is not exceeded while its mixing capability is guaranteed.[20] The optimal process temperature ranges were extracted from literature[21,22,23,24] or from the manufacturing data sheets. Depending on the polymer used, different extrusion temperatures were used, as listed in Table 1.

After extrusion, the filaments were collected on a self-winding roller and this roller speed was adapted to obtain filaments with a diameter of 1.75±0.05 mm as measured with a digital caliper. Filaments with a diameter out of this range were discarded.

Resulting filaments were stored in a dessicator containing silica, because absorbed moisture might lead to nozzle blockage or distortion of the printed part by formation of bubbles.[4]

2.3. Filament Characterization

2.3.1. Mechanical Testing

To evaluate the mechanical properties of the extruded filaments, samples were subjected to a tensile test in elongation mode using a TA.HD PlusC Texture analyser (Stable Micro Systems, UK) equipped with pneumatic clamps and a load cell of 50 kg. The specimen of 25 mm was elongated at a rate of 0.01 mm/sec until reaching a trigger force of 1g after which data collection started and the sample was further elongated at a rate of 0.02 mm/sec until 20% strain. Another specimen of 25 mm was subjected to elongation under the same conditions but with a tensile rate of 1 mm/sec until the maximum elongational distance of the machine was reached (300 mm). The curves of both tensile tests were compared to differentiate between polymers that broke during the test or could be maximally elongated. The Young's modulus, strain and stress at break and tensile energy to break the filament (area under the curve) were calculated as an average of five independent samples at low test speed using Matlab2018b. The Young's modulus was calculated as the slope between 0.05 and 0.25% strain in the stress-strain curve. These tensile test parameters were based on the ISO 527.[25]

2.3.2. Rheological analysis

A stress-controlled HAAKE Mars III rheometer (Thermo Scientific, Germany) equipped with a parallel plate geometry of 20 mm diameter and a Peltier temperature module was used. All rheological experiments were performed on small pieces of filaments as sample material which were stored in a desiccator until rheological analysis to prevent air bubbles due to moisture evaporation. After zero gap determination at the test temperature, samples were loaded and allowed to soften. The sample was trimmed and excess material was removed at a gap size of 1.1 mm. Samples were equilibrated at the measuring gap (1 mm) during 15 min prior to testing. A standard deviation of less than 5% was inferred for repeated experiments. Frequency sweeps were performed at 200, 180, 160 and 140 °C for all EVA/TPU grades and HPC EF. Frequency sweeps were performed at 120, 100, 80 and 60 °C for PEO and PCL. Frequency sweeps were performed at 100, 80 and 60 °C for PEO/PCL-IBU mixtures. Frequency and temperature sweeps were performed at a strain deformation of 1%, which proved to be within the linear viscoelastic region.

Validity of the Cox-Merz rule was assumed for pure polymers, as this empirical rule is obeyed rather well for a variety of polymers (unless very highly branched structures) with only minor deviations.[26] For polymers with high solid content, this rule may however not be applicable. The overlap of small amplitude oscillatory shear (SAOS) measurements with steady-state rotation shear (SSRS) was therefore investigated for the polymer-drug blends. SSRS experiments were conducted using rotational experiments in a shear rate range from 0.01 to 5 s^{-1}. During SAOS measurements, the complex viscosity (η^*) was measured in function of frequency (1-460 rad/s) at four different temperatures which were related to the printing temperature. The Cross model, as shown in Eq.(1)[27] was fitted to all frequency sweeps to determine the impact of these rheological parameters on the printing process.

$$\eta^*(\dot{\gamma}, T) = \frac{\eta_0}{1 + (\frac{\eta_0 \dot{\gamma}}{\tau^*})^{(1-n)}} \quad (1)$$

where τ^* is the critical shear stress at which the complex viscosity profile moves from Newtonian to shear thinning, n is the power-law index which accounts for the degree of shear-thinning and η_0 the zero-shear viscosity.

When the temperature of a frequency sweep is increased, the average relaxation time shortens due to an expansion of molecular mobility. This temperature dependency of η^* can be expressed by the time-temperature superposition principle. The storage modulus (G'), loss modulus (G") and η^* of four frequency sweeps were shifted to the frequency sweep of the third measured temperature (either 180°C or 80°C) using the TTS module of the HAAKE Rheowin software, resulting in a temperature-invariant mastercurve. From the obtained shift factors (aT), the Arrhenius flow activation energy (kJ.$K^{-1}.mol^{-1}$) was calculated, as shown in Eq. (2):[28]

$$E_a = \frac{R_G \ln aT}{\frac{1}{T} - \frac{1}{T_R}} \tag{2}$$

where R is the gas constant of 0.008314 kJ.$K^{-1}.mol^{-1}$, aT is the horizontal shift factor for a frequency sweep recorded at temperature T and T_R is the reference temperature at which the mastercurve is created.

Temperature sweeps were performed monitoring η^*, G' and G" in function of temperature, under a constant frequency of 6.28 rad/s. Samples were molten and equilibrated at either 200, 120 or 100 °C followed by a cooling run at 2 °C/min to either 80 °C or 25 °C. After solidification, a subsequent heating run at 2 °C/min was performed until the start temperature of the cooling run was reached. From this heating and cooling run, the temperature at the cross-over point (G'=G") was determined. At this point, the viscous and elastic properties of the material are equal which is important to predict the solidification behaviour of the formulation on the printer bed (cooling run) and the printing temperature (heating run).

2.3.3. Thermal analysis

The glass-transition temperature (T_g) and melting point(s) (T_m) of the polymers, blends and ibuprofen were evaluated using differential scanning calorimetry (DSC). The analysis was performed using Tzero pans (TA instruments, Belgium) in a DSC Q2000 (TA Instruments, UK) using a dry nitrogen flow rate of 50 mL/min. A heat-cool-heat run at heating/cooling rate of 10 °C/min was applied. Modulated DSC (mDSC) experiments were also performed in heating, with a heating rate of 2 °C/min. The modulation period and amplitude were set at 1 min and 0.32 °C, respectively (heat-iso method).

2.4. Tablet Printing

2.4.1. FDM desktop printer

The feedability of the filaments was tested on a Prusa i3 MK3S printer (Prusa Research, Prague) with a modified PTFE tube. The diameter of this tube was enhanced using a drill with diameter of 2.05 mm for the upper half and 1.95 mm for the lower half of the tube. Filaments that broke on or between the printing gears were labelled as ‘non-feedable’ as this impeded transport to the tube and hotend.

Feedable filaments were tested for their printability at different test temperatures and nozzle sizes (d = 0.4, 0.6 or 0.8 mm). In a first set of experiments, the flowability and feedability at different temperatures was assessed. Starting from 200 °C, the temperature was lowered in steps of 20 °C to establish at which temperature the flow out of the nozzle was blocked. The temperature at which this blockage occurs was determined on three different days to ensure the precision of the observed results. After determining this threshold, the print temperature was increased by 20 °C and objects were printed. The printed object was a cylindrical tablet with a diameter of 10 mm and height of 4 mm, layer height was 0.3 mm, 20% line infill, 2 shells and 2 top/bottom layers. The extrusion multiplier was set to 1. The first layer of the tablet was printed with a speed of 3 mm/s. A fan, blowing on the printed object, was disabled during the first layer and enabled at 100% of its maximum speed during the consecutive layers. The geometry of the printed part was designed as a .stl file using AutoCAD (Autodesk, USA) and converted into G-codes using Slic3r Prusa Edition software (Prusa Research, Prague). The platform temperature was kept constant at 30 °C. A certain set of conditions (temperature, speed, nozzle diameter) was deemed printable only if three consecutive tablets could be printed. When a tablet was printed with a speed of 90 mm/s, this will be referred to as the maximal printing speed as the printer can not accelerate up to this linear printing speed on such a small object, as was also discussed for other printers.[29] If printing with this speed was not possible, the print speed was consecutively decreased to 10 mm/s or 3mm/s. After the tablets were printed, the temperature was lowered by 20 °C to verify the minimal printing temperature. This large temperature step size ensures the robustness and precision of the method to estimate the minimal printing temperature. When filaments were changed, Klucel EF was fed at 200 °C, after which the nozzle was soaked in hot water.

The gap width between the gears of the Prusa i3 MK3S is user-controlled through a small screw connecting both sides of the feeding compartment. In this study, a maximal gap width was chosen to minimize the pressure exerted by the gears. However, small deviations in gap width might have occurred whenever the print head was reassembled after the cleaning procedure.

3. Results and Discussion

First the mechanical properties of the filaments are linked to their feeding behaviour and failure mechanisms (breakage or buckling). Secondly, the rheological behaviour of the filaments is discussed to investigate its influence on the printability and quality of the end-product. The individual rheological parameters also clarify the effect of nozzle diameter on the printing behaviour. Thirdly, the thermal behaviour of the filaments is linked to a specific failure mechanism, occurring only with the IBU-blends and EVA2825A. Finally, the effect of a crystallisation inhibitor (IBU) on the solidification behaviour of PEO and PCL is briefly discussed.

3.1. Feedability

Filament feedstock is pinched and pushed to the hotend in the printer head by means of a roller mechanism. The Prusa i3 MK3S is designed to have one stationary roller and one connected to a stepper motor. The motor-connected roller has a specific toothed surface to prevent slippage and create the necessary friction for successful feeding. The rollers pressurize the filament between them, which generally leads to a small deformation of the filament without impeding the mechanisms' feedability.[4] In some cases however, this way of feeding might result in feedability issues, rendering a filament non-printable. For example, it was observed in this study that Soluplus, KVA64 and Eudragit EPO could not be printed due to brittle failure. For SP60D60, SP93A, EVA1070 and EVA2825A process conditions had to be optimised as these filaments showed buckling behaviour. Both printing failure mechanisms will be discussed hereafter.

3.1.1. Brittle failure

The pressure between the print gears might exceed the material's ability to withstand the imposed stresses. In that case, the filament will shatter on the gears, thereby discontinuing the piston-action necessary for proper printing.[11] Filaments displaying this kind of failure (Soluplus, KVA64 and Eudragit EPO) are non-printable and it was not possible to print them, even when changing the process conditions (temperature, print speed or nozzle diameter) as the failure occurs before the filament enters the PTFE tube and liquefier. For example, similar results were obtained on a Makerbot Replicator 2, where KVA64 was too brittle to be printed successfully.[30] The addition of a plasticizer or a polymer with acceptable mechanical properties to these brittle filaments could however enable their printing. The addition of PEG 1500[31] or the addition of hydroxypropyl methylcellulose[30] to KVA64 for example, was already successful. In another study, the addition of 10% PEG to Soluplus enabled printing with this polymer.[11] The necessity of blending polymers or plasticizers with brittle matrices to enable their printing is a general phenomenon and was already investigated for a wide variety of polymers already, e.g. the addition of polylactic acid to poly-3-hydroxybutyrate (PHB)[32,33] or PEO to Eudragit EPO.[24]

The mechanical properties of the filament, measured by a tensile test, are predictive for this brittle feedability failure. When a filament could be stretched over the maximal length of the tensile testing apparatus (300 mm - 1mm/s) without breakage, it did not break on the printer gears either. This behaviour was exhibited by PCL, PCLIBU20, PCLIBU40 and the EVA/TPU grades. It should be noted that TPU EG72D could not be maximally elongated as the filament prematurely snapped from the pressurised clamps around 175-190 mm elongation. At this point, the maximal force exerted by the clamps was exceeded. All filaments were also subjected to a tensile test at low displacement rate to calculate their Young's modulus. The stress/strain at break and the tensile energy to break (the integrated area under the stress/strain curve)[34] of filaments breaking during the elongation test are displayed in Fig.1. It should be noted that the stress at break decreases for PEO with increasing drug content from 13.56

MPa (0% IBU) to 5.73 MPa (20% IBU) and 4.74 MPa (40% IBU), which is consistent with previous research and points out the plasticizing behaviour of IBU.[35] When grouping the filaments based on their printability outcome, filaments exhibiting low strain at break and low tensile energy to break are prone to fracture on the feeding gears. As can be seen in Fig.1, the threshold for printability based on the tensile energy to break is between 36,38 x 10^5 J/m^3 (PEO - printable) and 27,41 x 10^5 J/m^3 (Soluplus - non printable) and for strain at break between 59.45% (PEO - printable) and 26.01% (Soluplus - non printable). Stress at break was not a useful parameter as it could not differentiate between printable and non-printable filaments and also showed a large standard deviation for the brittle filaments. For example, the coefficient of variation for Soluplus is 16,87% compared to 4,63% for HPC EF. The tensile test is apparently not the ideal method to differentiate between feedable and non-feedable filaments based on the stress at break when highly brittle materials are examined. In this case, a compression test might be a better alternative. It was previously described before that small defects like cracks or cavities inside the sample weaken the filament in tensile mode, while their effect on compressive failure is less pronounced. As such the strength at break of a brittle filament might be higher in compressive mode, which reflects more accurately the printing process.[36] Such a compressive test is however not possible when flexible materials like TPUs or EVAs are included. In conclusion, the proposed simple and fast elongation method in the current research can be used as a fast screening tool for feedability, based on the energy to break the filament and the strain at break.

In previous studies, different kinds of mechanical tests were also investigated, for example three-point bend tests,[37] elongational tests,[38,39] resistance tests,[11] stiffness tests[40] or fracturability tests.[24] The exact lower limit of the parameters determined via these tests differs between studies as it also depends on the printers' mechanics and between different brands of printers. The general results from these tests are in accordance with each other and with the current research, showing that feeding failure occurs for filaments with high brittleness and that a high toughness and stiffness is desirable. In a recent study, an extensive comparison was made between a stiffness test, a resistance test and a three-point bend test which highlighted the discriminating potential of the stiffness test and the obtained thoughness value.[40] Sometimes, discrepancies between the outcome of a feedability test exist in literature. For example, PEO N10 was too fragile to be fed on a Makerbot printer in some studies,[41] while others successfully fed PEO N10 filaments.[11,42] Also, Eudragit EPO could be printed and did not break on the gears in a Makerbot Replicator 2X,[43] while the same polymer was non feedable in another study on the same printer.[11] These contradictions might arise from small adaptations of the printer by the user which might broaden the print window. It was shown for example that adaptation of a spring in the feeding mechanism of a Makerbot Replicator 2x reduced the compression forces on the feedstock material.[42] In the current research, the gap width between the gears is user-controlled and was also set at a maximum distance.

3.1.2. Buckling failure

Another prerequisite for a printable filament is its successful advancement from the gears towards the PTFE tube and nozzle. This process requires the filament to act as a piston to overcome the pressure drop of the system and push the melt out of the nozzle. This pressure drop depends on the feedstock viscosity, nozzle geometry and flow rate. The force needed to overcome this pressure is exerted on the filament by the gears and might cause buckling when a critical pressure (P_{cr}) is exceeded. This behaviour is described by the Euler buckling theory (Eq.(3)) and places limits on the feed rate and feedstock material properties.[4, 44, 45]

$$P_{cr} = \frac{\pi^2 E_Y d_f^2}{16 L_f^2} \tag{3}$$

where E_Y is the Young's modulus of the filament, d_f is the filament diameter and L_f is the filament length between the gears and the entrance of the PTFE tube. It must be noted that the Young's modulus in the Euler buckling theory refers to the compressive modulus. For most materials however, the initial part of the stress-strain curve is essentially the same in compression and tension.[36]

A filament suitable for 3D printing should have an acceptable stiffness (Young's modulus)[45, 38, 21] to overcome this critical pressure without buckling. Filaments with a low Young's modulus (Fig. 1), EVA1070 (77,1 MPa), EVA2825A (14,0 MPa), TPU SP60D60 (24,8 MPa) and TPU SP93A (14.46 MPa), showed buckling behaviour. A filament with low stiffness is challenging to print and its printability or possible process conditions strongly depend on its viscosity.[45] Optimisation of process conditions taking the viscosity into account might however enable printing of these elastic materials, as is discussed in the next section. It should be mentioned that it was not possible to print with EVA2825A, even with adapted process settings.

3.2. Printability

Printable filaments with their minimal printing temperature, cross-over point and melting point are mentioned in Table 2. At first, a comparison with literature in terms of printability and printing conditions for these polymers will be made for a nozzle size of ⌀0.4 mm. In the current research, printing of PCL was possible at 80 °C without speed restriction (90 mm/s). A number of previous studies reported printing of PCL e.g. at 100 °C and 45 mm/s (Makerbot 2),[22] at 90 °C and 180 mm/s (0.5 mm nozzle, Cobra printer),[46] at 100 °C and 90 mm/s (Makerbot 2X).[7] Printing of PEO was possible at 80 °C without speed restriction. A previous study reported printing of PEO N10 at 160 °C without mentioning the print speed (Makerbot).[42] Printing of the EVA-grades was possible at 160 °C and slow speed (10 mm/s) for EVA1070. With EVA2825A, printing failed repeatedly due to buckling of the filament. A previous study also investigated the use of EVA1070 with a Makerbot Replicator 2 and could only print this polymer at a higher temperature (210 °C) in combination with a low printing speed (10-35 mm/s).[22] To our knowledge, printing of EVA2825A was not reported in literature elsewhere. Printing of the TPUs was possible at 180 °C (EG72D, SP93A) or 160 °C (SP60D60). For SP93A, a very low printing speed (3 mm/s) had to be maintained. Printing of these TPUs was also investigated previously on a Makerbot Replicator 2X. For EG72D and SP60D60, printing was possible at approximately the same temperatures (180 and 150 °C respectively). For SP93A, a temperature of 150 °C was reported to provide sufficient flow out of the print nozzle, but it was stated that this filament was inadequate to prepare tablets because it was too soft for the printing gears.[21] It should however be noted that only a print speed of 90 and 150 mm/s was investigated by Verstraete et al. In the current research, printing of HPC EF was possible at 160 °C with no speed restriction. A previous study reported printing of HPC EF also at 160 °C at 90 mm/s, but with a bed temperature of 50 °C on a Makerbot Replicator 2X.[39] It must be noted that in the current research printing at a bed temperature of 30 °C was possible by reducing the distance between the nozzle and the bed, but a higher bed temperature indeed ameliorated the adhesion of the HPC EF tablet. Printing of IBU-loaded PEO and PCL was not possible in the current research at ⌀0.4. IBU was previously used as a model drug with PEO when starch (20% w/w) was added in the mixture and this blend was printable with a temperature of 165 °C and speed of 70 mm/s.[47] To our knowledge, no reports were made in literature where only IBU-loaded PCL or PEO was printed. Most of the mentioned research papers employed a Makerbot 2X to print these polymers into pharmaceutical dosage forms. In general, the printing temperatures mentioned in the current research are either comparable or lower than the ones reported previously, which might arise from a different hot-end set-up.

It can be seen in Table 2 that the minimal printing temperature for some matrices expands using a wider nozzle. No comparisons with literature for the other nozzle diameters could be made, as to our knowledge printing with these polymers at a nozzle size of ⌀0.6 or ⌀0.8 mm was not reported in literature elsewhere. It can also be noticed that process temperatures during extrusion-based 3D printing (Table 2) are generally higher compared to twin screw extrusion (Table 1), e.g. SP93A was extruded at (120 °C) and printed at (180 °C). This phenomenon is in accordance with previous reports.[48,30]

Based on their printing behaviour described in Table 2, the printable filaments can be categorized in simple and complex polymers. PEO and PCL can be classified as 'simple' polymers due to their linear molecular structure. The printing behaviour of pure PEO and PCL can easily be linked to their thermal and rheological behaviour. Their minimal printing temperature (80 °C) was close to the cross-over (62.2 and 58.7 °C respectively) and melting point (64.6 and 60.6 °C respectively) and does not change upon enlarging the nozzle diameter. The other filaments show a complexer behaviour, possibly due to their branched structure, and will be thoroughly characterized via rheological analysis. First, a link will be made with the Cross-model parameters. Secondly, the impact of the nozzle diameter on the printing behaviour is discussed in detail based on the Young's modulus, the pressure drop, volumetric flow and Arrhenius activation energy. A special case are the ibuprofen-loaded filaments, as they could only be printed using a larger nozzle diameter. This behaviour will be discussed under section 3.2.3 (Thermal behaviour).

3.2.1. Rheological behaviour: Cross-model parameters

The fitted Cross-model at different temperatures for EVA2825A is shown in Fig. S2. The Cross-model parameters at the minimal printing temperature are listed in Table 3 together with the R^2. These parameters were also normalized for PLA (200 °C) and PCL (80 °C), two frequently used polymers in extrusion-based 3D printing. This normalization aids in the direct comparison of the Cross-model parameters between different filaments. The chosen Cross-model describes both Newtonian and shear thinning behavior. It is hypothesised that an ideal filament for 3D printing consists of an early transition from Newtonian to shear thinning behaviour and exhibits a significant shear thinning behaviour. This would result in optimal flowability out of the nozzle. A high zero shear viscosity would also be beneficial to maintain the structure of the printed dosage form.[9,34] Should these hypothesises be true, an ideal filament bears a high η_0, low τ^* and high n value. However, from Table 3, it seems that the impact of these specific material parameters on the FDM 3D-printing processability with the Prusa i3 MK3S is limited. The variability of the model parameters between two simple, easily printable filaments (PCL, PEO) with comparable printing behaviour exceeds the variability between simple and complex polymers (TPUs, EVAs, HPC EF) or between complex polymers themselves. PCL has a high zero shear viscosity (4.18x10^4 Pa.s), low τ^* (5.70x10^3 Pa) and high n-value (0.473) which is characteristic of a Maxwellian behaviour (G'~w^2 and G"~w^1 at the low frequency region) as can be seen in Fig.3. As such, the melt closely resembles a viscous liquid with negligible elasticity. It In contrast, the moduli of PCL are less dependent on the angular frequency and thus the melt has a more distinct elastic behaviour. This polymer has a low zero shear viscosity (4.55x10^3 Pa.s), high τ^* (3.87x10^5 Pa) and low n-value (0.187). Such differences were previously correlated with printing quality as the print obtained from a Maxwellian polymer showed a marked decrease in visual quality.[49] In the current study however, such a distinct difference between the printing conditions or visual quality of prints from both polymers was not observed. As an explanation, one could say that FDM 3D printing is a complex process where there is a constant de- and accelaration of the print head and the flow continuously needs to stop and start. From this point of view, excessive shear thinning might negatively impact 3D printing. In addition, the Prusa i3 MK3S is equipped with a fan to cool the printed object. This fan also influences the printing behaviour and quality of the end-product, and broadens the window of printable materials. When tablets with PCL and PEO were printed with and without fan, a huge difference in quality of the end-product was observed. While a PCL tablet printed without fan showed warping and deformation, a PEO tablet printed without fan gave rise to a collapsed and deformed structure which lacked geometrical accuracy. In conclusion, while specific rheological model parameters are indispensable for flow model analysis, for the end-user these parameters can not be directly correlated to quantitative and qualitative differences in feeding and printing behaviour, at least for the materials investigated in this study.

Even though no relationship was detected between the rheological parameters and the printing behaviour, these parameters are of vital importance to describe and understand the printing process. For example, materials with a higher shear thinning behaviour or n-value showed less propensity to back-flow, which is the process where the molten material will move upwards inside the nozzle.[9,50] It was shown also that the flow in a hot-end nozzle is not continuous but rather turbulent and thus possesses a high degree of back-mixing. Due to back-mixing, the material has a broad residence time distribution within the nozzle, which intensifies the thermal load of the material.[29] As such, it might be possible that materials with a higher n-value show less back-flow and back-mixing which therefore reduces the thermal load of the API. Future research should be conducted to investigate this phenomenon.

Besides its importance to describe the flow behaviour of the printer, rheology is also indispensable to elucidate sources of printing defects. Printing quality was already correlated with rheological behaviour in SAOS experiments.[49] As can be seen in Fig. 2, certain defects in the PEO and PCL tablets can be explained by the rheological properties of the respective polymers. The cross-over point (G'=G") in cooling of PEO (45 °C) is closer to the printing temperature (80 °C) compared to PCL (31 °C). As a result, the polymer solidifies slightly faster after leaving the hot nozzle. When printing at the lowest print temperature, PEO solidified quickly, possibly resulting in incomplete welding of the individual layers. As a result, small gaps between infill and shell are visible. This effect is more pronounced at a larger nozzle diameter, due to a higher volumetric flow. For PCL, the cross-over point in cooling is lower as can be seen in Fig.2 As a result, solidification of the polymer takes longer compared to PEO. At a larger nozzle diameter, a visible collapse of the tablet structure is noticed, possibly due to the slower solidification which is more pronounced when the road width is increased (i.e. at larger nozzle diameter).

3.2.2. Impact of nozzle diameter

For the 'complex' materials (TPUs, EVAs and HPC EF), printing behaviour is influenced by the nozzle diameter of the printer as can be seen in Table 2. The minimal printing temperature drops and/or the maximal printing speed expands at a larger nozzle diameter, e.g. printing was possible with SP60D60 at 140 °C at nozzle size ⌀0.6 and ⌀0.8, while 160 °C was needed at ⌀0.4. For EG72D however, the print speed had to be reduced at ⌀0.8 compared with ⌀0.4 and ⌀0.6. To clarify all these effects, an estimation of the pressure drop over the nozzle and its influencing factors must be scrutinized. If this pressure drop is regarded as a simple Hagen-Poiseuille flow, it can be described by the following equation:[4]

$$\triangle P = \frac{8QL\eta}{\pi(\frac{D}{2})^4} \tag{4}$$

where △P is regarded as the pressure drop, Q as the volumetric flow rate, L the length over the nozzle, η the viscosity of the polymer melt and D the diameter of the nozzle opening. It must be noted that the Hagen-Poiseuille equation is only valid for Newtonian liquids. The expression becomes more complicated for polymeric melts obeying the Cross-model but still depends on the same variables - in addition to the parameters of the Cross-model. Using this (simplified) equation to describe the pressure drop over the nozzle, it becomes clear that the pressure drop depends on material properties (η), process variables (D,Q) and process constants (L) which only differ between printers.

Low Youngs' modulus. The materials with the lowest elasticity modulus (SP93A, SP60D60, EVA1070) were printable at a lower temperature or at a higher speed when a larger nozzle diameter was used. For SP93A and SP60D60 specifically, an increase in nozzle size from ⌀0.4 to ⌀0.6 lowered the minimal printing temperature from 180 to 160 °C and from 160 to 140 °C respectively. No further reduction was observed when using a ⌀0.8 nozzle. For EVA1070, no decrease in minimal printing temperature was observed. However, a faster printing speed could be applied with a ⌀0.6 or ⌀0.8 compared to a ⌀0.4 nozzle. Printing with EVA2825A was however not possible as it failed to print at each nozzle diameter. These effects can be explained by the variation in pressure drop, as a larger nozzle diameter reduced the pressure drop over the nozzle (Eq. (4)). This was also experimentally validated in previous research.[51] As described earlier by Eq (3), materials with a low elasticity modulus are sensitive to buckling behaviour. Accordingly, if the pressure drop over the nozzle is lower by enlarging the nozzle diameter, the critical pressure for buckling is higher.[52,51] As a result, the print window for a material with low elasticity modulus will enlarge at a higher nozzle diameter.

Pressure drop and maximal viscosity. The print window for EG72D and HPC EF also widens at larger nozzle diameters, although these polymers have a considerable elasticity modulus (442.2 MPa and 251.9 MPa, respectively). EG72D could be printed at a minimal temperature of 160 °C for nozzle size ⌀0.6 and ⌀0.8 compared with 180 °C for nozzle size ⌀0.4 but only at a very slow rate (3 mm/s). For HPC EF, printing temperature decreased from 160 to 140 °C when using a larger nozzle diameter. For these polymers, the effect of nozzle diameter is probably related to another mechanism than the earlier described Eulers' buckling theory and might result from a higher back pressure at lower nozzle diameters. This failure mechanism is related to processing highly viscous materials in a twin screw extruder. As melt viscosity and torque in a twin screw extruder are directly proportional, a high torque is required to rotate the screws with highly viscous materials.[6] Although no screw is present in a conventional filament-fed melt extrusion additive manufacturing process and the driving force required to push the melt from the nozzle depends solely on the pressure drop over the system.[4,53] The outcome of processing a highly viscous material is however similar: if the pressure drop or force to rotate the screws is excessive due to a high viscosity of the material, it might be impossible to generate the required torque by the motor in the 3D printer or twin screw extruder.[52] The generally accepted upper limit of viscosity in twin screw extrusion is 10,000 Pa.s.[20] Processing materials with a viscosity above this limit might cause torque overshoot and blocking of the extruder. The exact upper limit in melt extrusion additive manufacturing will mainly depend upon the used apparatus but is generally lower than the limit of hot melt extrusion, hence a higher processing temperature is generally required.[48,30] When excessive force is required to push the filament out of the nozzle, this results in a blocked nozzle and the filament in the feeding chamber will have a grinded surface due to the rotation of the toothed wheels.[54]

EG72D and HPC EF have indeed the highest viscosity-over-temperature profile (Fig. 4). Therefore, it is probably this high viscosity that limited their printing window. With the Prusa i3 MK3S, this upper limit was achieved at around ± 6,000 Pa.s for a nozzle of ⌀0.4 (Fig 4). In another study, the complex viscosity in a Makerbot printer should be below 8,000 Pa.s to enable sufficient flow out of the nozzle (⌀0.4 mm).[41] This again confirms that the existence of a viscosity limit is a general phenomenon but that the exact limits depend on the apparatus, as already described in other studies.[54] The upper viscosity limit shifted upwards (± 14,000 Pa.s) using a larger diameter nozzle (either ⌀0.6 or ⌀0.8) due to a decrease in pressure drop (Eq. 4). This shift will most likely also be a general phenomenon, independent of the used apparatus. In another study for example, the required extruder force was measured for a variety of build rates and nozzle diameters for various devices and it was shown that smaller nozzles require a higher extruder force to maintain the same build rate.[54]

Volumetric flow. Based on Eq. (4), the nozzle diameter should have a huge effect on the pressure drop (exponent of 4) and thus reduction in minimal printing temperature. The resulting drop in printing temperature is however not as dramatic as expected or even absent for some polymers (e.g. EVA1070). While enlarging the nozzle diameter could be beneficial to lower the minimal printing temperature, especially for drugs prone to thermal degradation, the maximally achieved difference in temperature is only 20 °C. In addition, it seems contradictory that EG72D (Table 2) has a drop in maximal printing speed (90 mm/s to 10 mm/s) at 180 °C when the nozzle size is expanded from ⌀0.4 to ⌀0.8.

These phenomena occur due to a limitation of the road width by the nozzle diameter, as the minimal road width is 1.2-1.5 times the nozzle opening.[55] As can be seen in Fig.(5), an expansion in nozzle diameter results in a broader road width even when the layer height is kept identical.[52,56] As a result, the volumetric flow rate must increase when a larger nozzle diameter is used with the same linear filament feed velocity, this results in an overall reduced build time of the object.[56] The linear feed velocity of the filament (v) depends on the volumetric flow rate from the nozzle (Q), road width (W) and layer height (h):[4]

$$v = \frac{Q}{Wh} \tag{5}$$

An increase in nozzle diameter reduces the pressure drop (Eq. 4) while at the same time this action is counteracted due to an increment in volumetric flow rate at the same linear speed. It is known that the process of heat transfer is often a limitation in the extrusion-based 3D printing process. Polymeric materials have a very low thermal conductivity, which is for example about 10,000 times lower than metals.[50] Due to this low thermal conductivity, temperature gradients exist inside the material during the melting process. These thermal gradients enlarge at higher feed rates due to a more restricted thermal penetration in the melt. As a result, the core temperature of the melt is lower at a higher volumetric feed rate and the required extrusion force increases.[54] The effect on the printing window in function of the nozzle diameter thus depends on a complex interplay of multiple factors which might counteract each other and is difficult to predict for each material individually. It is important to mention however that the higher volumetric flow rate due to nozzle enlargement can also reduce the residence time of the material inside the heated nozzle. It was shown for example that less back flow was observed when the nozzle size was widened from ⌀0.25 to ⌀0.4.[51] In conclusion, a decrease in residence time, together with the achieved lower printing temperature, might provide an interesting method to diminish degradation of the API.

Arrhenius activation energy. The differences in flow characteristics of the materials were further investigated by calculating the Arrhenius flow activation energies (Eq.2). This activation energy of flow is the energy needed to overcome the internal flow resistance and to achieve motion of the individual molecules.[57] The construction of a mastercurve by shifting individual frequency sweeps is displayed in Fig (S3). From these shift factors (aT), plots of ln(aT) in function of (1/T) were constructed (Fig.6) and the activation energy (E_a) could be calculated (Table 2). It was observed that TPU EG72D has the highest Arrhenius flow activation energy (114.03 kJ/mol), which might explain why the effect of nozzle enlargement has the largest influence on this polymer by limiting its maximal printing speed at ⌀0.8 to 10 mm/s at 180 °C. It shows that this polymer has a high flow retardation due to strong physcial crosslinks and intermolecular interactions.[34] It must be noted that for HPC EF the Arrhenius flow activation energy could not be calculated. For HPC EF, the time-temperature superposition (TTS) principle does not seem valid as the individual frequency sweeps did not superimpose, based on a van Gurp-Palmen plot (phase angle in function of the complex modulus). Probably, HPC EF is not a so-called thermorheological simple material, meaning that the relaxation mechanisms of the material have not the same temperature dependence. Especially for polydisperse samples, there is a gradual transition from one zone to another and it is impossible to place individual frequency sweeps on a master curve using a single value of aT.[58]

3.2.3. Thermal behaviour

For all blends containing ibuprofen, printing was challenging at nozzle size of ⌀0.4. Blends consisting of ibuprofen with PEO failed at all print temperatures due to deformation and melt compression of the filament at the roller gears. The filament was compacted and heavily deformed in the printing chamber (Fig. 7), which differs from the earlier described failure mechanisms (breakage, buckling or reaching the viscosity limit). The blend of 20% ibuprofen with PCL was printable at low speed (10 mm/s) from 80 °C onward, but it was difficult to print consecutive tablets under these conditions without observing the same failure phenomenon as with PEO.

The observed phenomenon could be related to a partial melting of the filament in the feeding chamber (Fig. S1) above the PTFE tube. This partial melting weakens the filament and enables grinding of the roller gears in the filament, which resulted in the observed defective feeding. This effect is probably present for the blends containing ibuprofen due to a decrease in melting temperature (Tm) of PCL and PEO with addition of IBU (Table 2). The drop in Tm occurs for both IBU-PCL and IBU-PEO but is more pronounced for the IBU-PEO mixtures. It demonstrates that IBU acts as a plasticizer and is well distributed and dissolved within the matrices,[59] which negatively impacts the feeding behaviour. In another study, indomethacin (30% w/w), blended with PEO N10, acted as a plasticizer and also rendered a non-printable formulation at a nozzle size of ⌀0.4.[40] In this current research however, feeding and printing of the IBU blends was possible and reproducible at a printing temperature of 60 °C with a nozzle size of ⌀0.6 and ⌀0.8. This is probably due to the earlier described drop in back pressure. Another example of the influence of an API on the thermal properties of a polymer was described for blends containing paracetamol and polyvinyl-alcohol. The Tg of the blends diminished at higher paracetamol content, hereby reducing the necessary temperature for twin-screw extrusion and extrusion-based 3D printing.[60]

As mentioned previously, printing was extremely difficult with EVA2825A. Next to its propensity to buckle (lowest Youngs' modulus of 14.0 MPa), it also has a low melting point, similarly as the IBU blends. The polymer was not at all printable at nozzle size ⌀0.4 and failed very often at nozzle sizes ⌀0.6 and 0.8. This combination of troublesome mechanical and thermal properties made this polymer not suitable for printing with the Prusa i3 MK3S.

3.3. Solidification behaviour and visual quality

After successful feeding and printing, the deposition on the build plate and solidification behaviour determines the visual quality of the tablet. As discussed previously, the addition of IBU to the PEO and PCL matrix decreased their melting temperature. For example, the melting point of PEO reduces from 64.6 °C to 56.3 °C at 20%w/w IBU and to 48.3 °C at 40%w/w IBU. The drug substance dissolves in the polymer matrices and acts as a plasticizer by expanding the free volume between the polymer chains.[15] This effect is also visible when comparing the viscosity ratio (η_0 drug loaded filament / η_0 pure polymer) (Table 4). The viscosity ratio at 60 °C for PEO blends with IBU decreases from 0.388 to 0.074 when the content of IBU is doubled from 20% to 40%. This shows that IBU increases the molecular mobility of the matrices. This effect is more pronounced at elevated temperature, for example, the viscosity ratio of PEO with 20% IBU lowers from 0.388 to 0.162 when the temperature rises from 60 °C to 80 °C. As a direct result of this increased molecular mobility, the minimal printing temperature of IBU-loaded filaments is lower compared to drug-free filaments. PEO with 20% IBU could be printed at 60 °C compared to 80 °C for the pure filament at a nozzle size of ⌀0.6. This effect was also seen with other drug-polymer combinations like ciprofloxacin-loaded polycaprolactone[16] and itraconazole-loaded hydroxypropyl methylcellulose acetaat.[61] Addition of the drug did not impede the applicability of the Cox-Merz rule for these polymer-drug dispersion, as there was an overlap of SAOS and SSRS measurements (Fig. 8).[17]

Fewer studies have included the effect of the solidification rate of a semicrystalline polymer on the quality of the end-product. It is known that a semicrystalline polymer is more difficult to print than an amorphous one, due to the shrinking and warping effect during crystallization. In order to obtain a strong 3D printed tablet, a process of welding or healing through molecular diffusion between two subsequent layers should take place.[50] Another prerequisite for a qualitative end-product is that strands should solidify quickly enough to support the weight of the subsequently deposited layer.[62] Therefore, in some cases it might be beneficial to add crystalline filler material that increase the overall viscosity and crystallisation rate of the polymer-drug melt, as this might enhance the visual quality of the product as was shown already by the addition of metoprolol tartrate to PCL.[39,15] The solidification behaviour of polymers is largely influenced by filler material, e.g. APIs that are either dispersed as crystals or dissolved. It was shown previously for example that ketoprofen dissolved in PEO, acted as a plasticizer and hence inhibited crystallization of the semi-crystalline matrix.[15] In conclusion, solidification behaviour is vital for high weld strength and high quality end-products in material extrusion.[46]

Influence of IBU on the solidification behaviour and visual quality of the end-product can be seen in Fig. 9. Pure PEO often shows voids between infill and shell due to insufficient welding. Addition of IBU lowers the cross-over point and overall viscosity during cooling, which improved the visual quality of the tablet. For example, the cross-over point during cooling decreases from 45.4 °C for pure PEO to 41.9 °C when 20% IBU is added and to 27.14 °C when 40% IBU is added. Indeed, when the viscosity of the melt flowing out of the nozzle is too high, poor bond quality can be observed as also discovered by Yang et al.,[35,63] and the addition of a viscosity-lowering agent might be beneficial in such occasions. However, when too much IBU is added, the visual quality of the end-product is worse. A similar effect was discovered when printing starch-based systems as a higher water content reduces the overall complex viscosity which hindered geometrical stability and softened the print.[64] A similar observation was made for amorphous polymers: printing of Eudragit EPO yielded a collapsed and deformed structure but addition of a filler (tricalcium phosphate) or an immiscible drug which remained crystalline in the blend (hydrochlorothiazide) increased the overall viscosity of the blend and the quality of the final dosage form.[43,65] The poorer tablet quality is possibly due to the large effect of IBU on the crystallization and solidification behaviour of PEO. A similar phenomenon occurs for PCL, as the tablet is easily deformed upon removal from the build platform and this effect is more pronounced when IBU is added. At the highest IBU concentration, the deformation of the tablet might even happen while printing.

4. Conclusion

The current research showed that specific material properties determine the 3D printability and optimal process parameters for a certain formulation. Filaments should possess a high toughness and stiffness with low brittleness in order to be feedable and compatible with the printers' gears. Secondly, if filaments are feedable, there is a complex interplay between their thermal, rheological and mechanical properties which determine the printability window. The minimal processing temperature for simple, linear materials depends mainly on the flow behaviour, indicating that the process temperature should exceed the melt and cross-over point. Filaments with low elasticity modulus and/or complex molecular structure show a more complicated printing behaviour. In general, enlarging the nozzle diameter of the printer reduces the minimal printing temperature, but this effect is (partially) counteracted by an increase of volumetric flow. Finally, a low melting point of the polymer could result in softening on the gears, which impedes successful feeding.

This study also investigated the effect of a plasticizing drug on the solidification behaviour of a polymer matrix and the resulting change in processability for material extrusion additive manufacturing and quality of the end-product. It was shown that ibuprofen acted as a plasticizer for PCL and PEO by decreasing the overall viscosity and the minimal printing temperature. Either the quality of the end-product was improved or over-plasticized structures were generated, depending on the ibuprofen content.

A comparison of this study with other research projects also pointed out that moving towards a generalised pharmaceutical, filament-free 3D printer would enlarge the portfolio of printable formulations and give rise to more consistent results in research.

5. Acknowledgements

The Paltel Group Foundation – Palestine is acknowledged for the funding of Aseel Samaro. The research project PRINTAID, the EU Framework Programme for Research and Innovation within Horizon 2020—Marie Sklodowska-Curie Innovative Training Networks under grant agreement No. 722467 is acknowledged for the funding of Bahaa Shaqour. Fundação para a Ciência e a Tecnologia, Lisboa, Portugal, is acknowledged for the PhD grant of Joana Macedo (SFRH/BD/125212/2016).

Furthermore, the authors would like to thank Kurt Van Houtte (Department of materials, Textiles and Chemical Engineering) for the adaptation of the Prusa Firmware to enable printing at low temperatures and prof. L. Cardon (Department of materials, Textiles and Chemical Engineering) for his useful input.

References

[1] Sarah J. Trenfield, Christine M. Madla, Abdul W. Basit, and Simon Gaisford. The shape of things to come: Emerging applications of 3D printing in healthcare. *AAPS Advances in the Pharmaceutical Sciences Series*, 31:1–19, 2018.

[2] Shaban A Khaled, Jonathan C Burley, Morgan R Alexander, Jing Yang, and Clive J Roberts. 3D printing of five-in-one dose combination polypill with defined immediate and sustained release profiles. 217:308–314, 2015.

[3] Christine M. Madla, Sarah J. Trenfield, Alvaro Goyanes, Simon Gaisford, and Abdul W. Basit. 3D printing technologies, implementation and regulation: An overview. *AAPS Advances in the Pharmaceutical Sciences Series*, 31:21–40, 2018.

[4] Brian N. Turner, Robert Strong, and Scott A. Gold. A review of melt extrusion additive manufacturing processes: I. Process design and modeling. *Rapid Prototyping Journal*, 20(3):192–204, 2014.

[5] Sisi Wang, Lore Capoen, Dagmar R. D'hooge, and Ludwig Cardon. Can the melt flow index be used to predict the success of fused deposition modelling of commercial poly(lactic acid) filaments into 3D printed materials? *Plastics, Rubber and Composites*, 47(1):9–16, 2018.

[6] Michael M. Crowley, Feng Zhang, Michael A. Repka, Sridhar Thumma, Sampada B. Upadhye, Sunil Kumar Battu, James W. McGinity, and Charles Martin. Pharmaceutical applications of hot-melt extrusion: Part I. *Drug Development and Industrial Pharmacy*, 33(9):909–926, 2007.

[7] Johanna Aho, Johan Peter Bøtker, Natalja Genina, Magnus Edinger, Lærke Arnfast, and Jukka Rantanen. Roadmap to 3D-Printed Oral Pharmaceutical Dosage Forms: Feedstock Filament Properties and Characterization for Fused Deposition Modeling. *Journal of Pharmaceutical Sciences*, 108(1):26–35, 2019.

[8] Hanna Ponsar, Raphael Wiedey, and Julian Quodbach. Hot-melt extrusion process fluctuations and their impact on critical quality attributes of filaments and 3d-printed dosage forms. *Pharmaceutics*, 12(6):1–15, 2020.

[9] Eric L. Gilmer, Darren Miller, Camden A. Chatham, Callie Zawaski, Jacob J. Fallon, Allison Pekkanen, Timothy E. Long, Christopher B. Williams, and Michael J. Bortner. Model analysis of feedstock behavior in fused filament fabrication: Enabling rapid materials screening. *Polymer*, 152:51–61, 2018.

[10] I. Gibson, D. W. Rosen, and B. Stucker. Extrusion-Based Systems. In *Additive Manufacturing Technologies: Rapid Prototyping to Direct Digital Manufacturing*, chapter 6, pages 143–169. Springer, New York, 2010.

[11] Jehad M. Nasereddin, Nikolaus Wellner, Muqdad Alhijjaj, Peter Belton, and Sheng Qi. Development of a Simple Mechanical Screening Method for Predicting the Feedability of a Pharmaceutical FDM 3D Printing Filament. *Pharmaceutical Research*, 35(8), 2018.

[12] Atheer Awad, Simon Gaisford, and Abdul W. Basit. Fused deposition modelling: Advances in engineering and medicine. In *AAPS Advances in the Pharmaceutical Sciences Series*, volume 31, chapter 6, pages 107–132. 2018.

[13] Moe Elbadawi, Brais Muñiz Castro, Francesca K.H. Gavins, Jun Jie Ong, Simon Gaisford, Gilberto Pérez, Abdul W. Basit, Pedro Cabalar, and Alvaro Goyanes. M3DISEEN: A novel machine learning approach for predicting the 3D printability of medicines. *International Journal of Pharmaceutics*, 590(August):119837, 2020.

[14] Witold Jamróz, Joanna Szafraniec, Mateusz Kurek, and Renata Jachowicz. 3D printing in pharmaceutical and medical applications. *Pharmaceutical Research*, 35(9):Article 176, 2018.

[15] Jeroen Van Renterghem, Chris Vervaet, and Thomas De Beer. Rheological Characterization of Molten Polymer-Drug Dispersions as a Predictive Tool for Pharmaceutical Hot-Melt Extrusion Processability. *Pharmaceutical Research*, 34(11):2312–2321, 2017.

[16] Moe Elbadawi, Thomas Gustaffson, Simon Gaisford, and Abdul W. Basit. 3D printing tablets: Predicting printability and drug dissolution from rheological data. *International Journal of Pharmaceutics*, 590(September):119868, 2020.

[17] Johanna Aho, Johan P. Boetker, Stefania Baldursdottir, and Jukka Rantanen. Rheology as a tool for evaluation of melt processability of innovative dosage forms. *International Journal of Pharmaceutics*, 494(2):623–642, 2015.

[18] Mohammad A. Azad, Deborah Olawuni, Georgia Kimbell, Abu Zayed Md Badruddoza, Md Shahadat Hossain, and Tasnim Sultana. *Polymers for extrusion-based 3D printing of pharmaceuticals: A holistic materials–process perspective*, volume 12. 2020.

[19] E Verhoeven, T R M De Beer, G Van Den Mooter, J P Remon, and C Vervaet. Influence of formulation and process parameters on the release characteristics of ethylcellulose sustained-release mini-matrices produced by hot-melt extrusion. *European Journal of Pharmaceutics and Biopharmaceutics*, 69:312–319, 2008.

[20] Simerdeep Singh Gupta, Tapan Parikh, Anuprabha K. Meena, Nidhi Mahajan, Imre Vitez, and Abu T.M. Serajuddin. Effect of carbamazepine on viscoelastic properties and hot melt extrudability of Soluplus®. *International Journal of Pharmaceutics*, 478(1):232–239, 2015.

[21] G Verstraete, A Samaro, W Grymonpre, V Vanhoorne, B Van Snick, M N Boone, T Hellemans, L Van Hoorebeke, J P Remon, and C Vervaet. 3D printing of high drug loaded dosage forms using thermoplastic polyurethanes. *International journal of pharmaceutics*, 536(1):318–325, jan 2018.

[22] Natalja Genina, Jenny Holländer, Harri Jukarainen, Ermei Mäkilä, Jarno Salonen, and Niklas Sandler. Ethylene vinyl acetate (EVA) as a new drug carrier for 3D printed medical drug delivery devices. *European Journal of Pharmaceutical Sciences*, 90:53–63, 2016.

[23] Kinga Ilyés, Norbert Krisztián Kovács, Attila Balogh, Enikő Borbás, Balázs Farkas, Tibor Casian, György Marosi, Ioan Tomuță, and Zsombor Kristóf Nagy. The applicability of pharmaceutical polymeric blends for the fused deposition modelling (FDM) 3D technique: Material considerations–printability–process modulation, with consecutive effects on in vitro release, stability and degradation. *European Journal of Pharmaceutical Sciences*, 129(January):110–123, 2019.

[24] Hazal Ezgi Gültekin, Serdar Tort, and Füsun Acartürk. An Effective Technology for the Development of Immediate Release Solid Dosage Forms Containing Low-Dose Drug: Fused Deposition Modeling 3D Printing. *Pharmaceutical Research*, 36(9), 2019.

[25] ISO. Plastics – Determination of tensile properties – Part 1: General principles. *527-1*, (527-1):13, 2006.

[26] Frank Snijkers and Dimitris Vlassopoulos. Appraisal of the Cox-Merz rule for well-characterized entangled linear and branched polymers. *Rheologica Acta*, pages 935–946, 2014.

[27] Timothy J. Coogan and David O. Kazmer. In-line rheological monitoring of fused deposition modeling. *Journal of Rheology*, 63(1):141–155, 2018.

[28] Thomas G Mezger. *The Rheology Handbook*, volume 38. 2009.

[29] Tim Feuerbach, Stefanie Kock, and Markus Thommes. Characterisation of fused deposition modeling 3D printers for pharmaceutical and medical applications. *Pharmaceutical Development and Technology*, 23(10):1136–1145, 2018.

[30] Nayan G. Solanki, Md Tahsin, Ankita V. Shah, and Abu T.M. Serajuddin. Formulation of 3D Printed Tablet for Rapid Drug Release by Fused Deposition Modeling: Screening Polymers for Drug Release, Drug-Polymer Miscibility and Printability. *Journal of Pharmaceutical Sciences*, 107(1):390–401, 2018.

[31] Gayathri Kollamaram, Denise M. Croker, Gavin M. Walker, Alvaro Goyanes, Abdul W. Basit, and Simon Gaisford. Low temperature fused deposition modeling (FDM) 3D printing of thermolabile drugs. *International Journal of Pharmaceutics*, 545(1-2):144–152, 2018.

[32] S Wang, K De Clerck, and L Cardon. Polylactic acid poly-3-hydroxybutyrate applications in Extrusion based Additive Manufacturing. *International Conference on Polymers and Moulds Innovations*, pages 1–5, 2018.

[33] Sisi Wang, Lode Daelemans, Rudinei Fiorio, Maling Gou, Dagmar R. D'hooge, Karen De Clerck, and Ludwig Cardon. Improving mechanical properties for extrusion-based additive manufacturing of poly(lactic acid) by annealing and blending with poly(3-hydroxybutyrate). *Polymers*, 11(9):1–13, 2019.

[34] Ngoc A. Nguyen, Christopher C. Bowland, and Amit K. Naskar. A general method to improve 3D-printability and inter-layer adhesion in lignin-based composites. *Applied Materials Today*, 12(May):138–152, 2018.

[35] Yan Yang, Huihui Wang, Haichao Li, Zhimin Ou, and Gensheng Yang. 3D printed tablets with internal scaffold structure using ethyl cellulose to achieve sustained ibuprofen release. *European Journal of Pharmaceutical Sciences*, 115(September 2017):11–18, 2018.

[36] Ferdinand P (Late of Lehigh University) Beer, E. Russel (Late of University of Connecticut) Johnston, John T. (University of Connecticut) DeWolf, and David F (United States Coast Guard Academy) Mazurek. *Mechanics of Materials*. McGraw-Hill Education, seventh ed edition, 2015.

[37] Jiaxiang Zhang, Xin Feng, Hemlata Patil, Roshan V. Tiwari, and Michael A. Repka. Coupling 3D printing with hot-melt extrusion to produce controlled-release tablets. *International Journal of Pharmaceutics*, 519(1-2):186–197, 2017.

[38] Alvaro Goyanes, Usanee Det-Amornrat, Jie Wang, Abdul W. Basit, and Simon Gaisford. 3D scanning and 3D printing as innovative technologies for fabricating personalized topical drug delivery systems. *Journal of Controlled Release*, 234:41–48, 2016.

[39] A. Samaro, P. Janssens, V. Vanhoorne, J. Van Renterghem, M. Eeckhout, L. Cardon, T. De Beer, and C. Vervaet. Screening of pharmaceutical polymers for extrusion-Based Additive Manufacturing of patient-tailored tablets. *International Journal of Pharmaceutics*, 586(June), 2020.

[40] Pengchong Xu, Jiangwei Li, Alvin Meda, Frederick Osei-Yeboah, Matthew L. Peterson, Michael Repka, and Xi Zhan. Development of a quantitative method to evaluate the printability of filaments for fused deposition modeling 3D printing. *International Journal of Pharmaceutics*, 588(August):119760, 2020.

[41] Abdullah Isreb, Krzysztof Baj, Magdalena Wojsz, Mohammad Isreb, Matthew Peak, and Mohamed A. Alhnan. 3D printed oral theophylline doses with innovative 'radiator-like' design: Impact of polyethylene oxide (PEO) molecular weight. *International Journal of Pharmaceutics*, 564(April):98–105, 2019.

[42] Alice Melocchi, Federico Parietti, Alessandra Maroni, Anastasia Foppoli, Andrea Gazzaniga, and Lucia Zema. Hot-melt extruded filaments based on pharmaceutical grade polymers for 3D printing by fused deposition modeling. *International Journal of Pharmaceutics*, 509(1-2):255–263, 2016.

[43] Muzna Sadia, Agata Sośnicka, Basel Arafat, Abdullah Isreb, Waqar Ahmed, Antonios Kelarakis, and Mohamed A. Alhnan. Adaptation of pharmaceutical excipients to FDM 3D printing for the fabrication

of patient-tailored immediate release tablets. *International Journal of Pharmaceutics*, 513(1-2):659–668, 2016.

[44] N. Venkataraman, S. Rangarajan, M.J. Matthewson, B. Harper, A. Safari, S.C. Danforth, G. Wu, N. Langrana, S. Guceri, and A. Yardimci. Feedstock material property – process relationships in fused deposition of ceramics (FDC). *Rapid Prototyping Journal*, 6(4):244–253, 2000.

[45] Jintian Wu, Ning Chen, Feng Bai, and Qi Wang. Preparation of Poly (vinyl alcohol)/ Poly (lactic acid)/ Hydroxyapatite Bioactive Nanocomposites for Fused Deposition Modeling. *Polymer composites*, 2018.

[46] Lily Northcutt, Kalman Migler, and Anthony Kotula. Crystallization Kinetics during Materials Extrusion based Additive Manufacturing of Polycaprolactone. *Annual Technical Conference - ANTEC, Conference Proceedings*, 2018-May, 2018.

[47] Touraj Ehtezazi, Marwan Algellay, Yamir Islam, Matt Roberts, Nicola M. Dempster, and Satyajit D. Sarker. The Application of 3D Printing in the Formulation of Multilayered Fast Dissolving Oral Films. *Journal of Pharmaceutical Sciences*, 107(4):1076–1085, 2018.

[48] Bahaa Shaqour, Aseel Samaro, Bart Verleije, Koen Beyers, and Chris Vervaet. Production of Drug Delivery Systems Using Fused Filament Fabrication : A Systematic Review. *Pharmaceutics*, 12:1–16, 2020.

[49] Gianluca Cicala, Davide Giordano, Claudio Tosto, Giovanni Filippone, Antonino Recca, and Ignazio Blanco. Polylactide (PLA) filaments a biobased solution for additive manufacturing: Correlating rheology and thermomechanical properties with printing quality. *Materials*, 11(7), 2018.

[50] Michael E. Mackay. The importance of rheological behavior in the additive manufacturing technique material extrusion. *Journal of Rheology*, 62(6):1549–1561, 2018.

[51] H. S. Ramanath, C. K. Chua, K. F. Leong, and K. D. Shah. Melt flow behaviour of poly-ϵ-caprolactone in fused deposition modelling, 2008.

[52] Brian N. Turner and Scott A. Gold. A review of melt extrusion additive manufacturing processes: II. Materials, dimensional accuracy, and surface roughness. *Rapid Prototyping Journal*, 21(3):250–261, 2015.

[53] Anna Bellini, Selcuk Guceri, and Maurizio Bertoldi. Liquefier Dynamics in Fused Deposition. *Journal of Manufacturing Science and Engineering*, 126(2):237, 2004.

[54] Jamison Go, Scott N Schiffres, Adam G Stevens, and A John Hart. Rate limits of additive manufacturing by fused filament fabrication and guidelines for high-throughput system design. *Additive Manufacturing*, 16:1–11, 2017.

[55] Mukesh K Agarwala. Structural quality of parts processed by fused deposition. Rapid Prototyping Journal. pages 4–19, 1996.

[56] Meng sha Huang, Min Zhang, and Bhesh Bhandari. Assessing the 3D Printing Precision and Texture Properties of Brown Rice Induced by Infill Levels and Printing Variables. *Food and Bioprocess Technology*, 12(7):1185–1196, 2019.

[57] G. Toth, D. Nagy, A. Bata, and K. Belina. Determination of polymer melts flow-activation energy a function of wide range shear rate. *Journal of Physics: Conference Series*, 1045(1), 2018.

[58] Donald Plazek and John Dealy. Time-temperature superposition-a users guide. *Rheology Bulletin*, 78 (2)(January 2009):16–31, 2009.

[59] G. V. Salmoria, F. Sibilia, V. G. Henschel, S. Fare, and M. C. Tanzi. Structure and properties of polycaprolactone/ibuprofen rods prepared by melt extrusion for implantable drug delivery. *Polymer Bulletin*, 74(12):4973–4987, 2017.

[60] J. Macedo, A. Samaro, V. Vanhoorne, C. Vervaet, and J.F. Pinto. Processability of poly (vinyl alcohol) Based Filaments With Paracetamol Prepared by Hot-Melt Extrusion for Additive Manufacturing. *Journal of Pharmaceutical Sciences*, 109:3636–3644, 2020.

[61] Nayan G. Solanki, Suhas G. Gumaste, Ankita V. Shah, and Abu T.M. Serajuddin. Effects of Surfactants on Itraconazole-Hydroxypropyl Methylcellulose Acetate Succinate Solid Dispersion Prepared by Hot Melt Extrusion. II: Rheological Analysis and Extrudability Testing. *Journal of Pharmaceutical Sciences*, 108(9):3063–3073, 2019.

[62] Katarzyna Pietrzak, Abdullah Isreb, and Mohamed A. Alhnan. A flexible-dose dispenser for immediate and extended release 3D printed tablets. *European Journal of Pharmaceutics and Biopharmaceutics*, 96:380–387, 2015.

[63] Camden A. Chatham, Callie E. Zawaski, Daniel C. Bobbitt, Robert B. Moore, Timothy E. Long, and Christopher B. Williams. Semi-Crystalline Polymer Blends for Material Extrusion Additive Manufacturing Printability: A Case Study with Poly(ethylene terephthalate) and Polypropylene. *Macromolecular Materials and Engineering*, 304(5):1–11, 2019.

[64] Ahmed Raouf Fahmy, Thomas Becker, and Mario Jekle. 3D printing and additive manufacturing of cereal-based materials: Quality analysis of starch-based systems using a camera-based morphological approach. *Innovative Food Science and Emerging Technologies*, 63(January):102384, 2020.

[65] Muzna Sadia, Abdullah Isreb, Ibrahim Abbadi, Mohammad Isreb, David Aziz, Amjad Selo, Peter Timmins, and Mohamed A. Alhnan. From 'fixed dose combinations' to 'a dynamic dose combiner': 3D

printed bi-layer antihypertensive tablets. *European Journal of Pharmaceutical Sciences*, 123(July):484–494, 2018.

Table 1: Overview of the extrusion temperature for all filaments.

Matrix	**T(extr)** °C	**T(die)** °C
SP60D60	150	130
SP93A	120	100
EG72D	180	160
EVA1070	120	120
EVA2825A	100	100
HPC EF	150	120
PEO	70	65
IBUPEO20	65	50
IBUPEO40	65	50
PCL	80	70
IBUPCL20	75	60
IBUPCL40	50	50

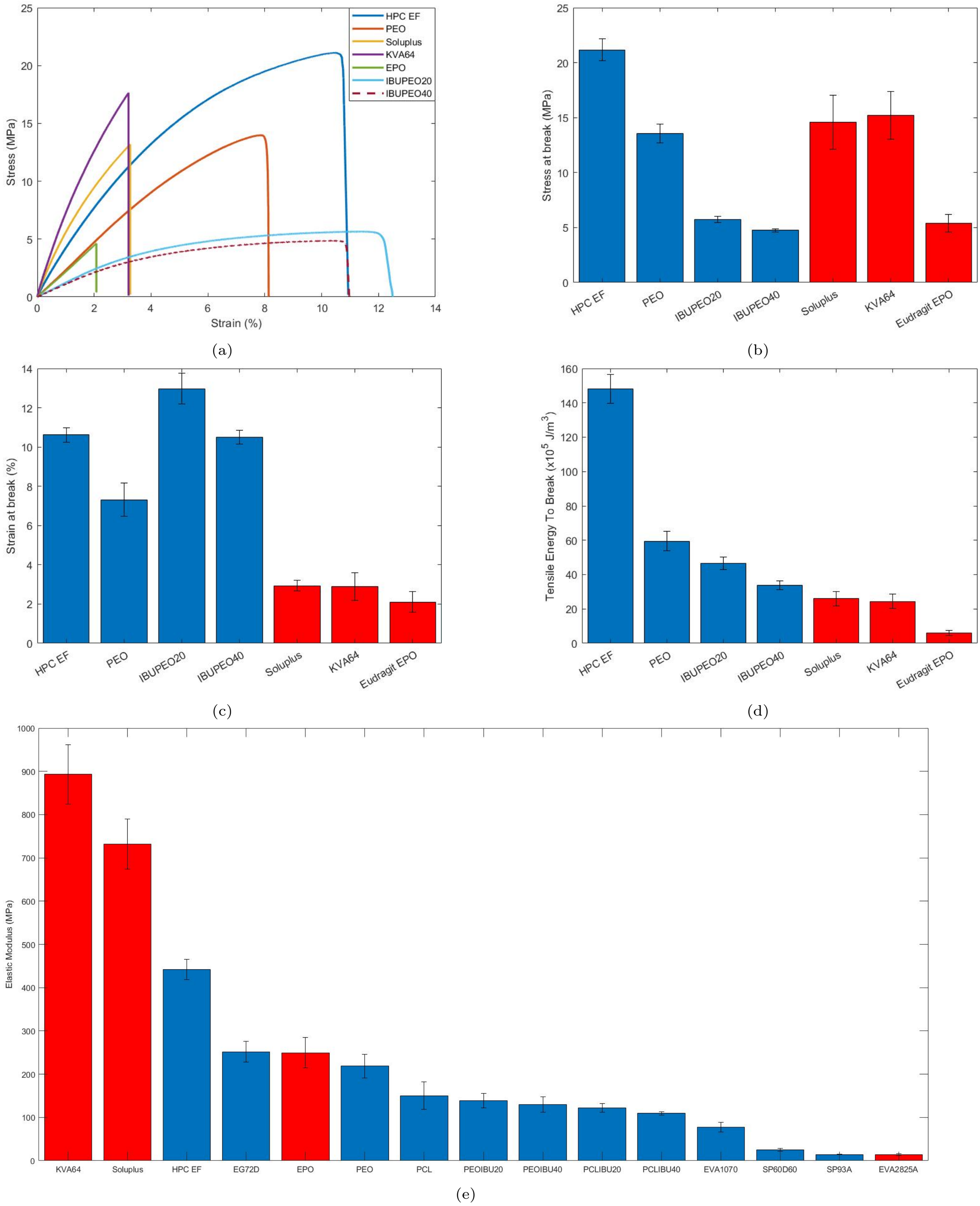

Figure 1: (a) The stress-strain curves of the filaments that broke during the tensile test at low displacement rate. (b) The stress at the breaking point, (c) the strain at the breaking point and (d) the respective tensile energy to break these filaments.(e) The Young's modulus of all filaments, measured as the initial straight part of the stress-strain curve at the lowest displacement rate. Red colored bars represent filaments which were not printable, in contrast to the blue colored bars.

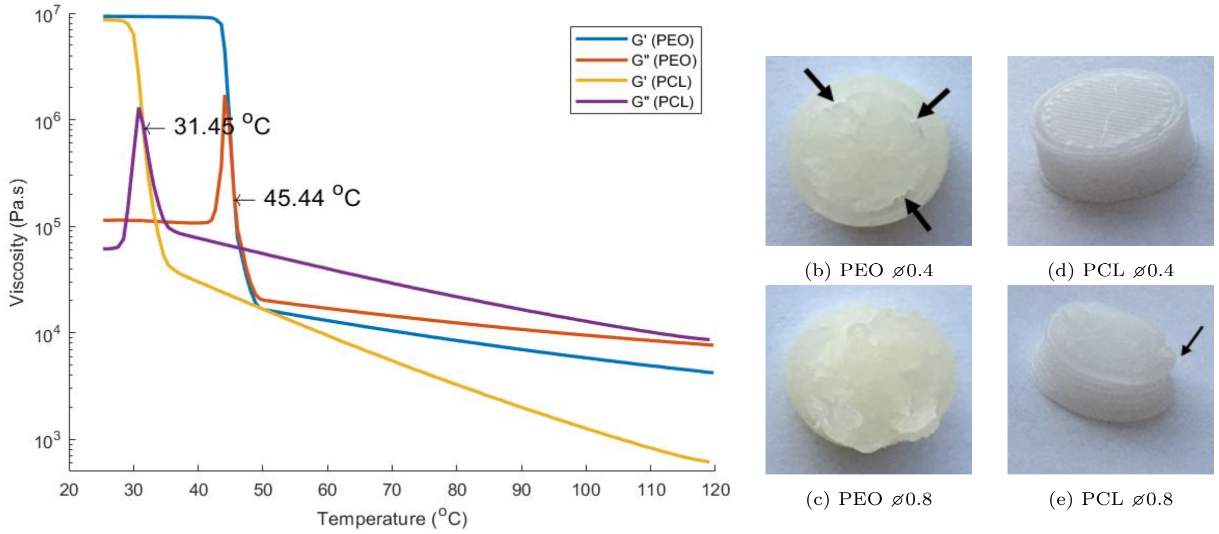

(a) Cross-over point (G'=G") for PEO and PCL.

(b) PEO ⌀0.4 (d) PCL ⌀0.4

(c) PEO ⌀0.8 (e) PCL ⌀0.8

Figure 2: Defects in shape or surface of the printed tablets can be attributed to certain rheological properties and differences. (a) Cross-over temperatures for PEO and PCL. (b-c) Tablets of PEO were printed at 80 °C with different nozzle sizes (⌀0.4 or 0.8) showing the incomplete welding behaviour (black arrows) at lower nozzle diameter. (d-e) Tablets of PCL were printed at 80 °C with different nozzle sizes (⌀0.4 or 0.8) showing the deformation of the PCL tablet at higher nozzle diameter (black arrow).

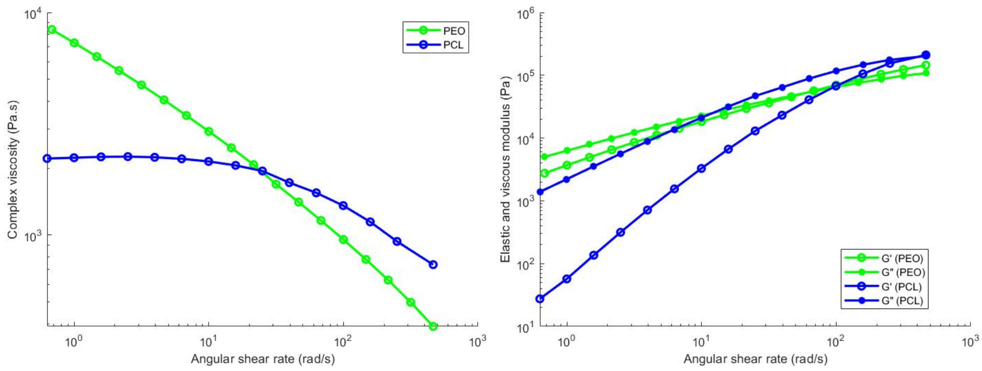

(a) (b)

Figure 3: (a) Complex viscosity for PEO (green) and PCL (blue) (b) Elastic (G', open symbols) and viscous (G", closed symbols) moduli for PEO (green) and PCL(blue). PCL shows Maxwellian behaviour while PEO displays a more distinctive elastic behaviour.

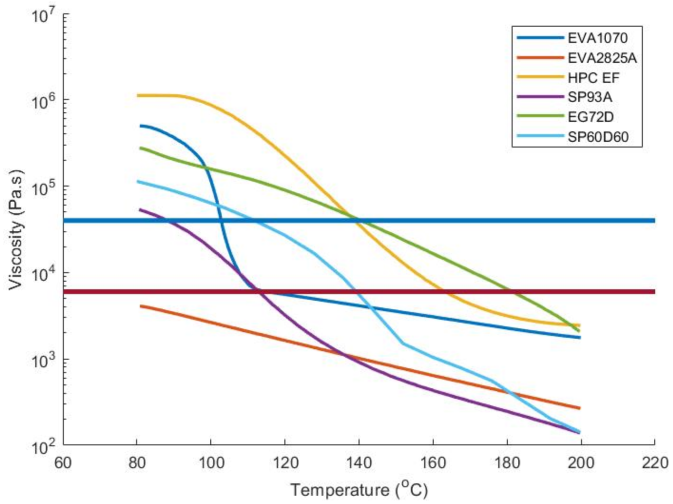

Figure 4: Complex viscosity as a function of temperature during a heating sweep. Red line represents the estimated maximal viscosity at nozzle size ⌀0.4 for a Prusa i3 MK3S system, above which printing is not possible. With higher nozzle diameter, maximal viscosity is assumed to shift towards a higher value as indicated by the blue line.

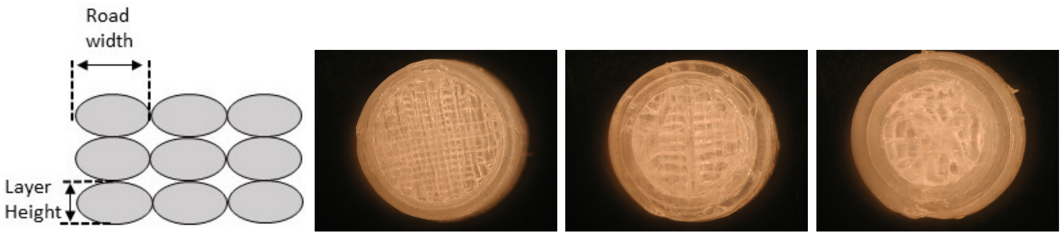

(a) (b) (c) (d)

Figure 5: (a) A simplified illustration of the structure of a 3D printed object (cross-section), showing road width and layer height. (adapted from[52]) (b-d) Top views of HPC EF tablets printed with consecutive nozzle sizes ⌀0.4, ⌀0.6 and ⌀0.8. Note the visible enlargement of road width with increasing nozzle diameter.

Table 2: Printable filaments with their minimal printing temperatures at different nozzle diameters and their material properties (melting point, cross-over point in heating). The maximal printing speed at different nozzle diameters is also reported. When no print speed is mentioned, the tablet was printed at the maximal printing speed of the printer (90 mm/s in the slicer), which is far above the actual speed the printer will attain when printing the tablet.

	Minimal print temperature			**Material properties**		
	⌀0.4	⌀0.6	⌀0.8	T_m	$T_{G'=G"}$	Ea
Matrix	°C	°C	°C	°C	°C	kJ/mol
PEO	80	80	80	64.6	62.2	44.77
PCL	80	80	80	60.6	58.7	34.17
SP60D60	160	140	140	61.7, 128.9	131.5	73.46
SP93A	180 (3 mm/s)	160	160	7.9, 43.6	106.2	66.44
				72.8, 126.2		
EG72D	180	160 (3 mm/s)	160 (3 mm/s)	63.1	137.5	114.03
		180	180 (10 mm/s)			
EVA1070	160 (10 mm/s)	160	160	98.4	152.4	47.69
EVA2825A	/	/	/	47.6, 72.9	68.1	52.82
HPC EF	160	140	140	186.8	187.7	n.a.
IBUPCL20	/	60	60	55.2	53.3	38.72
IBUPCL40	/	60	60	52.9	50.5	46.88
IBUPEO20	/	60	60	56.3	56.8	38.58
IBUPEO40	/	60	60	48.3	50.9	37.63

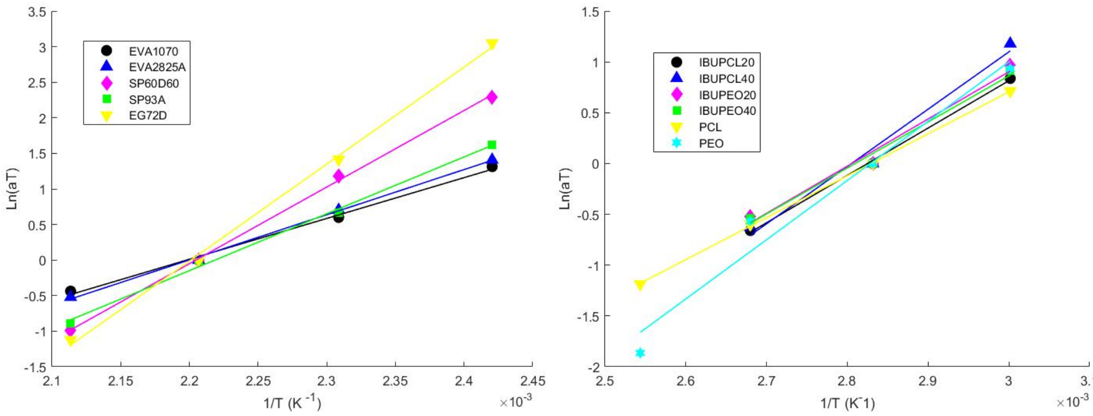

(a) (b)

Figure 6: Shift factor (aT) as a function of the inverse temperature (1/T) obtained from the master curve construction. The Arrhenius fit was performed at 180°C (a) or 80°C (b).

Table 3: Cross-model parameters of frequency sweeps at the minimum printing temperature (left) and normalized with the model parameters of either PLA (200 °C or PCL (80 °C (right). A large variability between parameters of the different filaments at their respective minimal printing temperature is shown. For EVA2825A, the parameters at 180 °C are shown instead of at the minimal printing temperature as this polymer was not printable.

	Print temperature (⌀0.4 mm)				Normalized for PLA (200 °C)		
Matrix	η_0 **(Pa.s)**	τ^* **(Pa)**	**n**	R^2	η_0 **(Pa.s)**	τ^* **(Pa)**	**n**
SP60D60	2.03×10^3	3.29×10^5	0.204	0.9995	0.81	4.62	0.48
SP93A	5.18×10^2	2.14×10^5	0.397	0.9941	0.21	3.01	0.93
EG72D	8.41×10^3	2.67×10^5	0.317	0.9997	3.34	3.75	0.74
EVA1070	2.95×10^4	3.23×10^3	0.476	0.9996	11.72	0.05	1.12
EVA2825A*	5.65×10^2	1.37×10^4	0.404	0.9991	0.22	0.19	0.95
HPC EF	5.16×10^5	1.64×10^3	0.329	0.9999	205.07	0.02	0.77
	Print temperature (⌀0.6 mm)				Normalized for PCL (80 °C)		
PEO	4.18×10^4	5.70×10^3	0.473	0.9998	9.19	0.01	2.53
IBUPEO20	1.62×10^4	4.07×10^3	0.503	0.9998	3.56	0.01	2.69
IBUPEO40	3.08×10^3	4.60×10^3	0.461	0.9998	0.68	0.01	2.47
PCL	4.55×10^3	3.87×10^5	0.187	0.9996	1.00	1.00	1.00
IBUPCL20	3.26×10^3	2.73×10^5	0.168	0.9991	0.72	0.71	0.90
IBUPCL40	1.43×10^3	1.54×10^5	0.164	0.9989	0.31	0.40	0.88

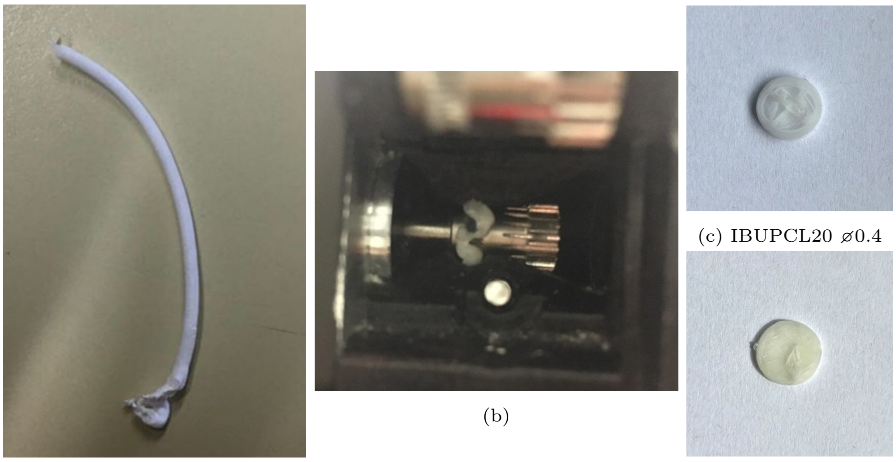

(a) (b) (c) IBUPCL20 ⌀0.4 (d) IBUPEO20 ⌀0.4

Figure 7: Melt compression failure occurs when printing with IBU mixtures, giving rise to deformation of the filament (a) between the gears of the enclosed printing chamber (b). With IBUPCL, printing with ⌀0.4 was possible but failure mid-print occurred regularly (c) With IBUPEO, printing with ⌀0.4 almost never gave a completed tablet (d).

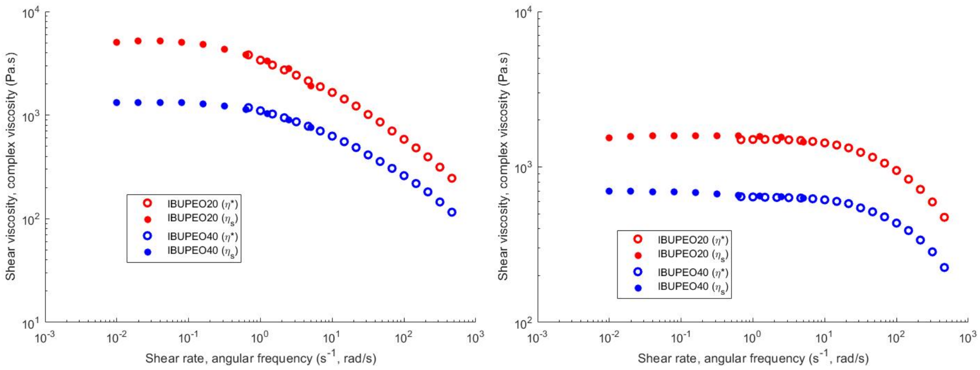

(a) (b)

Figure 8: Shear viscosity (η_s) as a function of shear rate (SSRS) and complex viscosity (η^*) as a function of angular frequency (SAOS) for (a) IBUPEO blends and (b) IBUPCL blends at 80^{o}C, showing applicability of the Cox-Merz rule for the drug-polymer dispersions.

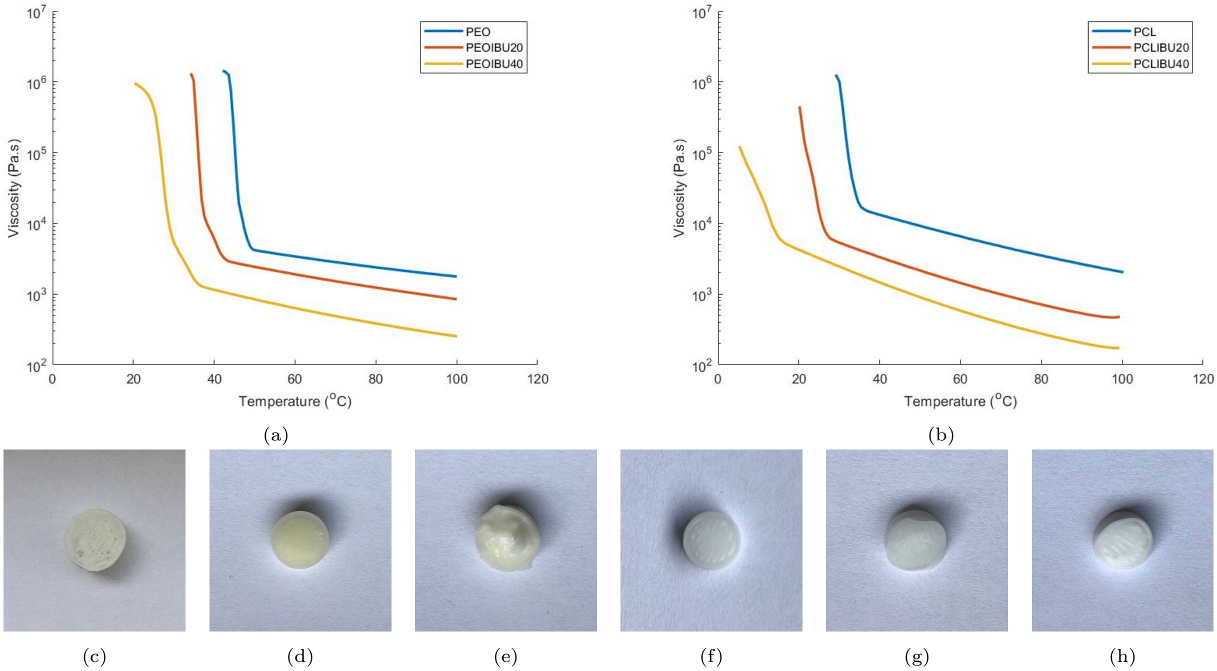

Figure 9: Complex viscosity as a function of temperature during a cooling run for PEO (a) and PCL (b) with 20 or 40% ibuprofen. (c-e) PEO tablets printed at 80 °C, nozzle size ⌀0.6 with increasing ibuprofen content from left to right (c 0%, d 20%, e 40%). (f-h) PCL tablets printed at 80 °C, nozzle size ⌀0.6 with increasing ibuprofen content from left to right (f 0%, g 20%, h 40%).

Table 4: Viscosity ratio of PCL and PEO in function of the ibuprofen concentration (% w/w).

		Drug concentration	
Polymer	**T** (°C)	**20 %**	**40 %**
PEO	60	0.388	0.074
	80	0.162	0.040
PCL	60	0.716	0.314
	80	0.336	0.143

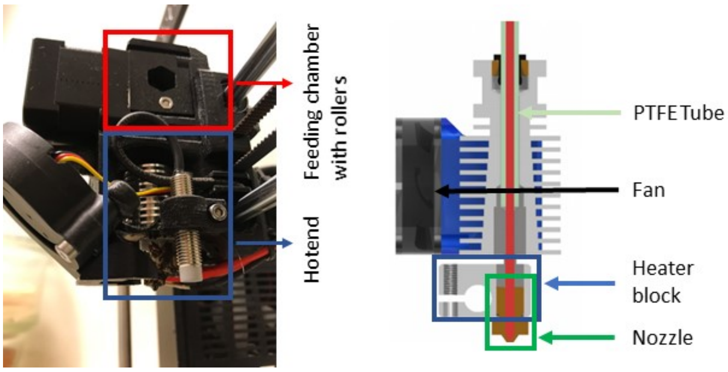

(a) (b)

Figure S1: (a) Overview of the Prusa MK3S with feeding chamber and hotend. (b) Detailed cross-section of the E3D V6 hotend.

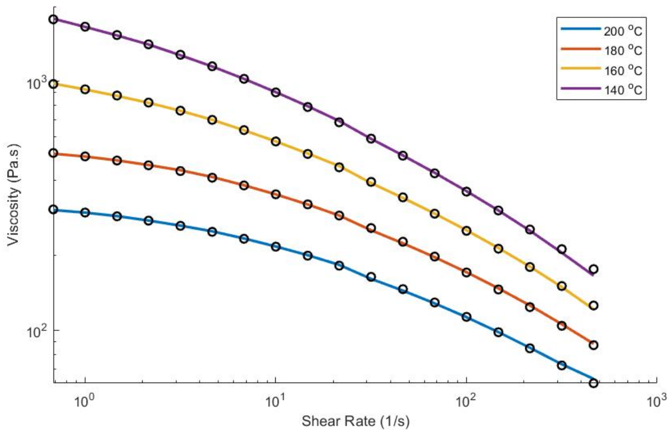

(a)

T	Cross-model parameters		
	η_0	τ^*	n
140 °C	2.28×10^3	1.16×10^4	0.430
160 °C	1.13×10^3	1.22×10^4	0.425
180 °C	5.65×10^2	1.37×10^4	0.404
200 °C	3.26×10^2	1.12×10^4	0.403

(b)

Figure S2: (a) Viscosity versus shear rate at four temperatures for EVA2825A. Lines indicate the experimental data, while the superimposed dots represent points predicted by the applied Cross-model. (b) Specific Cross-model parameters at each temperature for EVA2825A.

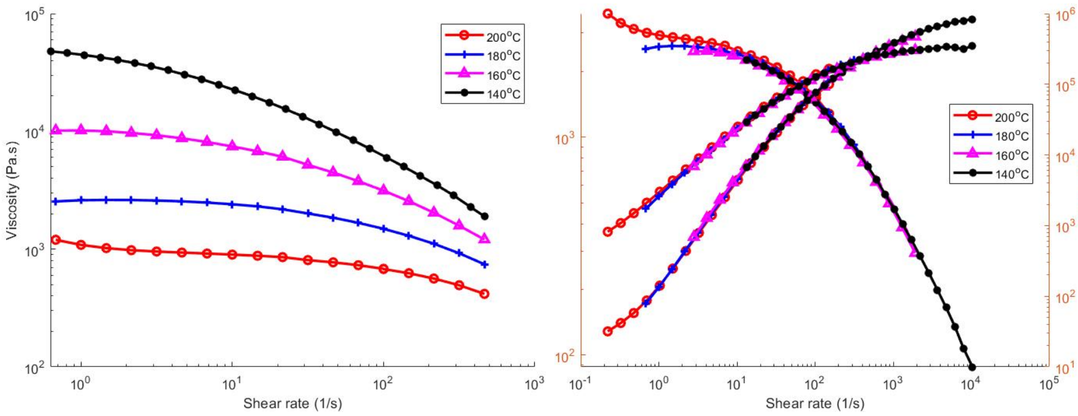

(a) (b)

Figure S3: Complex viscosity as a function of angular frequency for TPU EG72D at different temperatures (a). Master curve at 180 °C by shifting complex viscosities, G' and G" of individual frequency sweeps (b).

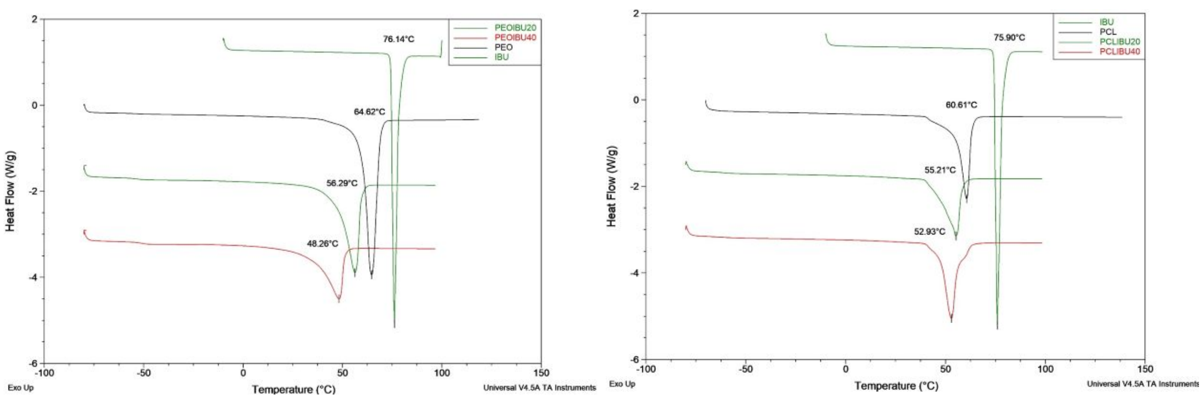

(a) (b)

Figure S4: DSC thermograms of IBU-PEO (a) and IBU-PCL (b) extrudates in a first heating scan. A shift towards lower melting temperature is visible upon increase of the IBU content within the filament.